Arch. Mech., **67**, 1, pp. 95–109, Warszawa 2015

Brief Note

A note on finite elastic deformations of fibre-reinforced non-linearly elastic tubes

M. EL HAMDAOUI, J. MERODIO

Department of Continuum Mechanics and Structures
Universidad Politécnica de Madrid
28040, Madrid, Spain
e-mail: merodioj@gmail.com

A fibre-reinforced non-linearly elastic tube subject to a finite radially symmetric deformation given by the combination of axial stretch, radial deformation and torsion is analysed. The deformation is supported by axial load, internal pressure and end moment. The materials at hand are neo-Hookean models augmented with a function that accounts for the existence of a unidirectional reinforcement. This function endows the material with its anisotropic character and is referred to as a reinforcing model. The nature of the considered anisotropy has a particular influence on the shear response of the material, in contrast to previous analyses in which the reinforcing model was taken to depend only on the stretch in the fibre direction. Furthermore, the ellipticity analysis of the deformations at hand has been carried out. It is shown that most of the deformations are non-elliptic, which opens the possibility to discontinuous solutions.

Key words: fibre-reinforced materials, finite deformations, ellipticity.

1. Introduction

In a recent paper El Hamdaoui *et al.* [1] examined extension, inflation and torsion of a tube in the context of non-linear elasticity theory. The strain energy (constitutive equation) was given in terms of an isotropic base material augmented by a function that accounts for the existence of a unidirectional reinforcement. Two independent invariants are sufficient to characterise the anisotropic nature of a transversely isotropic material model (such as a fibre-reinforced material): one is related directly to the fibre stretch and is denoted by I_4; the other invariant, denoted by I_5, is also related to the fibre stretch but introduces an additional effect that is related to the behaviour of the reinforcement under shear deformations (see Merodio and Ogden [2]). Here, our purpose is to investigate a neo-Hookean material reinforced with a function that depends on I_5, taken as a quadratic model, and to compare the results with those given by El Hamdaoui *et al.* [1] for the corresponding I_4 reinforcement. In addition, we include here the analysis of loss of ellipticity that determines both the *deformation* associated with the existence of surfaces of weak discontinuity and the *direction of the normal* to that surface (see Merodio and Neff [3], Merodio and Ogden [4]). The ellipticity analysis provides light on the application of this study since it deals with the analytical solution of the problem at hand.

The so-called standard reinforcing model is a quadratic function that depends only on I_4. It has been widely investigated in the last few years with application to the behaviour of rubber-like materials as well as to soft tissue in biomechanics. The same is not the case for the invariant I_5 for which there are only a few studies available in the literature.

In most of the cases, for the loading conditions at hand the fibre reinforcement is under compression. Compressive failure of fibre composites which consist of an isotropic base material includes fibre kinking and fibre splitting (see Lee *et al.* [5]). In this paper, our objective is to present, in the setting of non-linear elasticity theory, the material instabilities mentioned above for the particular fibre-reinforced materials at hand. Surfaces of weak discontinuity (or weak surfaces) are surfaces across which the second derivative of the displacement field is discontinuous, while across a fully developed (or strong) surface of discontinuity the first derivative (i.e., the deformation gradient) suffers a finite jump.

The torsion of isotropic incompressible materials has been studied by many authors in many papers since the pioneering work of Rivlin and Saunders [6], among others, as well as the simultaneous extension, inflation and torsion, see for instance, Rivlin and Saunders [6], Gent and Rivlin [7], Kanner and Horgan [8], Horgan and Polignone [9] and references therein. Combined extension and inflation of such materials including bifurcation into non-circular cylindrical modes of deformation has been presented by Haughton and Ogden [10] and Merodio and Haughton [11]. An extension to fibre-reinforced materials of that analysis has been given by Rodríguez and Merodio [12].

In Section 2, we study the basic equations we are using following El Hamdaoui *et al.* [1]. Main results are described in Section 3 for the model at hand, a neo-Hookean material augmented with a reinforcement that depends on the invariant I_5. The ellipticity analysis is carried out in Section 4 and main conclusions of the study are written in Section 5.

2. Preliminaries

2.1. Kinematics and constitutive model

Let $\mathbf{X}$ denote the position vector of a material particle in the stress-free reference configuration and $\mathbf{x}$ denote the corresponding position vector in the deformed configuration. The deformation gradient tensor is denoted $\mathbf{F}$ and has components $\partial x_i/\partial X_\alpha$. The left and right Cauchy-Green deformation tensors, respectively $\mathbf{B}$ and $\mathbf{C}$, are given by

$$\mathbf{B} = \mathbf{F}\mathbf{F}^{\mathrm{T}}, \qquad \mathbf{C} = \mathbf{F}^{\mathrm{T}}\mathbf{F}, \tag{2.1}$$

and the principal (isotropic) invariants of $\mathbf{C}$ (equivalently of $\mathbf{B}$) are defined by

$$I_1 = \operatorname{tr}\mathbf{C}, \qquad I_2 = I_3 \operatorname{tr}(\mathbf{C}^{-1}), \qquad I_3 = \det\mathbf{C}. \tag{2.2}$$

In terms of the principal stretches $(\lambda_1, \lambda_2, \lambda_3)$ of the deformation we have

$$I_1 = \lambda_1^2 + \lambda_2^2 + \lambda_3^2, \quad I_2 = I_3(\lambda_1^{-2} + \lambda_2^{-2} + \lambda_3^{-2}), \quad I_3 = \lambda_1^2\lambda_2^2\lambda_3^2. \tag{2.3}$$

We consider a fibre reinforcement identified in the undeformed configuration by the unit vector $\mathbf{M}$. The combination of $\mathbf{M}$ and $\mathbf{C}$ introduces two additional invariants, denoted I_4 and I_5, which are defined by

$$I_4 = \mathbf{M}\cdot(\mathbf{C}\mathbf{M}), \qquad I_5 = \mathbf{M}\cdot(\mathbf{C}^2\mathbf{M}). \tag{2.4}$$

Let the vector $\mathbf{m}$, resulting from the action of $\mathbf{F}$ on $\mathbf{M}$, be $\mathbf{m} = \mathbf{F}\mathbf{M}$. In this paper we focus on *incompressible* elastic materials, so that $I_3 \equiv 1$ and hence

$$\lambda_1\lambda_2\lambda_3 = 1. \tag{2.5}$$

The most general incompressible non-linearly elastic material is given by the strain energy function

$$W = W(I_1, I_2, I_4, I_5), \tag{2.6}$$

and the corresponding Cauchy stress tensor is given by

$$\sigma = \mathbf{F}\frac{\partial W}{\partial \mathbf{F}} - p\mathbf{I}, \tag{2.7}$$

where the parameter p denotes the Lagrange multiplier arising from the incompressibility constraint.

Using (2.2), (2.4), (2.6) and (2.7), one can write

$$\begin{aligned} \sigma = 2W_1\mathbf{B} + 2\,W_2\,(I_1\mathbf{I} - \mathbf{B})\mathbf{B} + 2\,W_4\,\mathbf{m}\otimes\mathbf{m} \\ + 2\,W_5\,(\mathbf{m}\otimes\mathbf{B}\mathbf{m} + \mathbf{B}\mathbf{m}\otimes\mathbf{m}) - p\mathbf{I}, \end{aligned} \tag{2.8}$$

where $\mathbf{I}$ is the identity tensor and the notation $W_i = \partial W/\partial I_i$, $i \in \{1, 2, 4, 5\}$ has been used. Furthermore, in the stress-free reference configuration, where $I_1 = I_2 = 3$ and $I_4 = I_5 = 1$, it follows that

$$W = 0, \qquad 2W_1 + 4W_2 = p_0, \qquad W_4 + 2W_5 = 0, \tag{2.9}$$

where p_0 is the value of p evaluated in the reference configuration.

2.2. Deformation

We now describe the basic equations of the deformation. Consider a right circular cylindrical shell that occupies the region

$$A \leq R \leq B, \qquad 0 \leq \Theta \leq 2\pi, \qquad 0 \leq Z \leq L, \tag{2.10}$$

in its undeformed reference configuration where (R, Θ, Z) are cylindrical coordinates. The position vector of a material point can then be written

$$\mathbf{X} = R\,\mathbf{E}_R(\Theta) + Z\,\mathbf{E}_Z, \tag{2.11}$$

where $\mathbf{E}_R$, $\mathbf{E}_\Theta$ and $\mathbf{E}_Z$ are unit vectors in the indicated directions.

The cylinder is inflated, extended and twisted so that it remains a circular cylinder. The inflating pressure is denoted by P, the axial load by N and the twist moment by M. In this deformed configuration the cylinder is described by

$$\mathbf{x} = r\,\mathbf{e}_r(\theta) + z\,\mathbf{e}_z, \qquad a \leq r \leq b, \qquad 0 \leq \theta \leq 2\pi, \qquad 0 \leq z \leq \ell, \tag{2.12}$$

where r, θ and z are cylindrical coordinates that are defined by

$$r = r(R), \qquad \theta = \Theta + \tau\lambda_z Z, \qquad z = \lambda_z Z, \tag{2.13}$$

respectively. The deformation gradient takes the form

$$\mathbf{F} = \lambda_r\,\mathbf{e}_r \otimes \mathbf{E}_R + \lambda_\theta\,\mathbf{e}_\theta \otimes \mathbf{E}_\Theta + \lambda_z\,\mathbf{e}_z \otimes \mathbf{E}_Z + \lambda_z\gamma\,\mathbf{e}_\theta \otimes \mathbf{E}_Z, \tag{2.14}$$

in which $\gamma = \tau r$ is being used. The incompressibility constraint $\lambda_r\lambda_\theta\lambda_z = 1$ leads to the connection

$$r^2 - a^2 = \lambda_z^{-1}(R^2 - A^2). \tag{2.15}$$

The tensors given in (2.1) using (2.14) are easily written as

$$\begin{aligned} \mathbf{C} &= \lambda_r^2\,\mathbf{E}_R \otimes \mathbf{E}_R + \lambda_\theta^2\,\mathbf{E}_\Theta \otimes \mathbf{E}_\Theta + \lambda_z^2(1+\gamma^2)\,\mathbf{E}_Z \otimes \mathbf{E}_Z \\ &\quad + \gamma\lambda_z\lambda_\theta\,(\mathbf{E}_\theta \otimes \mathbf{E}_Z + \mathbf{E}_Z \otimes \mathbf{E}_\Theta), \\ \mathbf{B} &= \lambda_r^2\,\mathbf{e}_r \otimes \mathbf{e}_r + (\lambda_\theta^2 + \gamma^2\lambda_z^2)\,\mathbf{e}_\theta \otimes \mathbf{e}_\theta + \lambda_z^2\,\mathbf{e}_z \otimes \mathbf{e}_z \\ &\quad + \gamma\lambda_z^2\,(\mathbf{e}_\theta \otimes \mathbf{e}_z + \mathbf{e}_z \otimes \mathbf{e}_\theta). \end{aligned} \tag{2.16}$$

Using $(2.16)_1$, (2.4) and (2.2) it is convenient to introduce a new function, denoted $\bar{W}$, such that

$$W = W(I_1, I_2, I_4, I_5) = \bar{W}(\lambda_\theta, \lambda_z, \gamma). \tag{2.17}$$

In summary, under the conditions at hand λ_z is fixed and the (local) simple shear deformation occurs in planes $(\mathbf{E}_\Theta, \mathbf{E}_Z)$, normal to $\mathbf{E}_R$. Furthermore, the quantities λ_θ and λ_z associated with the azimuthal and axial directions are not, in general, the principal stretches of the deformation. In particular, we have such a case only in the absence of torsional deformation, corresponding to $\gamma = 0$.

2.3. Equilibrium

In the absence of body forces the equilibrium equations can be written (see [1]) as

$$r\frac{d}{dr}(\sigma_{rr}) + \sigma_{rr} - \sigma_{\theta\theta} = 0, \qquad \frac{d}{dr}(r^2\sigma_{r\theta}) = 0, \qquad \frac{d}{dr}(r\sigma_{rz}) = 0. \tag{2.18}$$

We further consider the radial boundary conditions

$$\sigma_{rr} = \begin{cases} -P & \text{on} \quad r = a, \\ 0 & \text{on} \quad r = b \end{cases} \tag{2.19}$$

which together with the integral of $(2.18)_1$ give

$$P = \int_a^b (\sigma_{\theta\theta} - \sigma_{rr})\frac{dr}{r}. \tag{2.20}$$

Now, a direct integration of $(2.18)_{2,3}$ gives

$$\sigma_{r\theta} = \frac{c_1}{r^2}, \qquad \sigma_{rz} = \frac{c_2}{r}, \tag{2.21}$$

where c_1 and c_2 are two constants. The two solutions given in (2.21) are not generally compatible with the specific forms of $\sigma_{r\theta}$ and σ_{rz} that arise from the constitutive law. This will be clarified later after (3.5) and (3.6).

The axial load and the resultant moment are given by

$$N = \int_a^b \int_0^{2\pi} \sigma_{rr} r \, d\theta dr \qquad \text{and} \qquad M = \int_a^b \int_0^{2\pi} \sigma_{\theta z} r^2 \, d\theta dr, \tag{2.22}$$

respectively.

Using $\bar{W}$, it is possible to write, after some manipulations (see [1])

$$\begin{aligned} P &= \int_a^b \left(\lambda_\theta \frac{\partial \bar{W}}{\partial \lambda_\theta} + \gamma \frac{\partial \bar{W}}{\partial \gamma}\right) \frac{dr}{r}, \\ N_r = N - \pi a^2 P &= \pi \int_a^b \left(2\lambda_z \frac{\partial \bar{W}}{\partial \lambda_z} - \lambda_\theta \frac{\partial \bar{W}}{\partial \lambda_\theta}\right) r dr - \frac{3}{2}\tau M, \\ M &= 2\pi \int_a^b \frac{\partial \bar{W}}{\partial \gamma} r^2 dr. \end{aligned} \tag{2.23}$$

Now, using $\lambda_r\lambda_\theta\lambda_z = 1$ and (2.15) one can write

$$\frac{dr}{r} = \left(1-\lambda_\theta^2\lambda_z\right)^{-1}\frac{d\lambda_\theta}{\lambda_\theta}. \tag{2.24}$$

It follows that it is possible to change the independent variable from r to λ_θ in (2.23). We also note that (2.24) and $(2.23)_{1,2}$ particularized for $\tau = 0$ yield the results established in [10] and [11] for the case of extension and inflation.

3. A neo-Hookean transversely isotropic material model

We focus now on the strain energy function

$$W = \frac{\mu}{2}\left[I_1 - 3 + \rho(I_5-1)^2\right], \tag{3.1}$$

where $\mu > 0$ is the constant representing the shear modulus of the base (isotropic) material in the undeformed configuration and $\rho > 0$ is a constant related to the degree of anisotropy. The isotropic material is the neo-Hookean model while the fibre contribution is given by the anisotropic invariant I_5 (see Merodio and Ogden [13]). Using (2.8) and (3.1) one can write

$$\boldsymbol{\sigma} = 2W_1\mathbf{B} + 2\,W_5\left(\mathbf{m}\otimes\mathbf{Bm} + \mathbf{Bm}\otimes\mathbf{m}\right) - p\mathbf{I}. \tag{3.2}$$

The fibre direction $\mathbf{M}$ is

$$\mathbf{M} = M_R\mathbf{E}_R + M_\Theta\mathbf{E}_\Theta + M_Z\mathbf{E}_Z. \tag{3.3}$$

Now, the anisotropic invariants I_4, I_5 upon use of $(2.16)_1$, (2.14) and (2.4) for the given direction $\mathbf{M}$ are

$$\begin{aligned} I_4 &= \lambda_r^2 M_R^2 + (\lambda_\theta M_\Theta + \gamma\lambda_z M_Z)^2 + \lambda_z^2 M_Z^2,\\ I_5 &= \lambda_r^4 M_R^2 + \lambda_\theta^2(\lambda_\theta^2+\gamma^2\lambda_z^2)M_\Theta^2 + 2\gamma\lambda_\theta\lambda_z(\lambda_\theta^2+\lambda_z^2+\gamma^2\lambda_z^2)M_\Theta M_Z\\ &\quad + \lambda_z^2[\gamma^2\lambda_\theta^2 + (1+\gamma^2)^2\lambda_z^2]M_Z^2. \end{aligned} \tag{3.4}$$

The components $r\theta$ and rz of the Cauchy stress tensor (3.2) using $(2.16)_2$, (2.14) and (3.3) can be written as

$$\begin{aligned} \sigma_{r\theta} &= 2\lambda_r M_R W_5\{\lambda_\theta M_\Theta(\lambda_r^2+\lambda_\theta^2+\gamma^2\lambda_z^2)\\ &\qquad + \gamma\lambda_z M_Z(\lambda_r^2+\lambda_\theta^2+\lambda_z^2(\gamma^2+1))\}, \end{aligned} \tag{3.5}$$

$$\sigma_{rz} = 2\lambda_r M_R W_5\{\gamma\lambda_\theta\lambda_z^2 M_\Theta + \lambda_z M_Z(\lambda_r^2+\lambda_z^2(\gamma^2+1))\}. \tag{3.6}$$

It follows that none of these components is consistent with (2.21), unless $M_R = 1$ and $M_\Theta = M_Z = 0$ or $M_R = 0$ when they both vanish and $c_1 = c_2 = 0$.

Therefore, we focus our attention on these special fibre geometries $M_R = 1$ and $M_R = 0$. For these two cases the considered deformation is controllable and also relative-universal in the full class of transversely isotropic elastic materials, for each case separately (see [1]).

For the model at hand, as opposed to the work developed in [1], expressions for P^*, M^* and N_r^* given by

$$P^* = \frac{P}{\mu}, \qquad M^* = \frac{M}{\pi\mu A^3}, \qquad N_{\mathrm{r}}^* = \frac{N - \pi a^2 P}{\pi\mu A^2}, \tag{3.7}$$

cannot be obtained explicitly. Whence, in the Sections that follow, we consider for the tube geometry, the material and the axial stretch the parameters given in Table 1 together with a variety of values of the twist parameter τ.

Table 1. Numerical parameters for the tube geometry (A and B), the material (ρ) and the axial stretch (λ_z).

A	B	ρ	λ_z
1	2	2	1.2

3.1. Radial transverse isotropy $M_R = 1$

First, we consider the case of transverse isotropy in the radial direction, for which $M_R = 1$ and $M_\Theta = M_Z = 0$. It follows using (3.4) that $I_4 = \lambda_r^2$ and $I_5 = I_4^2$. The latter identity establishes that under these circumstances the results are qualitatively similar to the results given in [1]. Nevertheless, we provide some numerical results to assess the analytical methodology described. In particular, for $\rho = 2$ and $\lambda_z = 1.2$ results are shown in Fig. 1 for a series of values of τ.

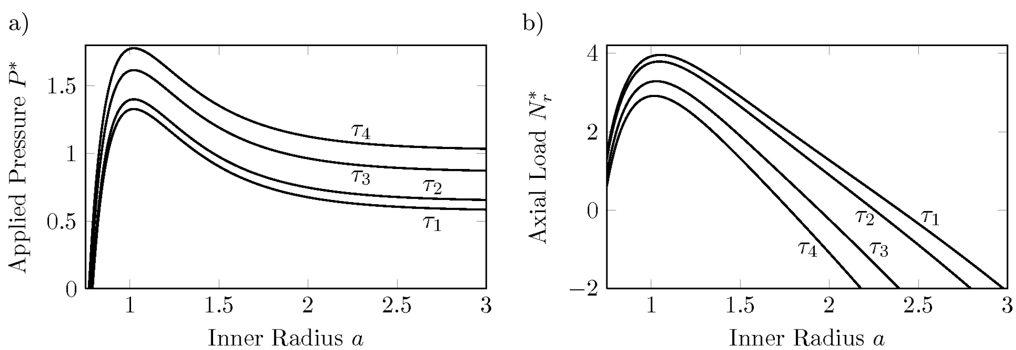

FIG. 1. For the case of radial transverse isotropy the dimensionless pressure P^*, given in (a), and reduced axial load N_r^*, given in (b), are plotted against the inner radius a for the following values of the dimensionless torsional strain $\tau_{1,2,3,4} = (0,\ 0.2,\ 0.4,\ 0.5)$.

The curves in each plot of Fig. 1 show the same qualitative behaviour for different values of the dimensionless torsional strain τ. In particular, the curves in the left plot show that the dimensionless pressure P^* has a maximum, i.e., for a given value of τ values of P^* increase up to a maximum and then decrease down to a (more or less) constant value for a plateau of values of a. For a given value of a, greater values of τ are associated with greater values of P^*. On the other hand, in the right plot, the curves show that the dimensionless reduced axial load N_r^* has a maximum, i.e., values of N_r^* increase up to a maximum and then decrease. For a given value of a, greater values of τ are associated with smaller values of N_r^*.

3.2. Transverse isotropy $M_R = 0$

The direction $\mathbf{M}$ for a general (helical) transverse isotropy is characterized by

$$\mathbf{M} = \cos(\alpha)\,\mathbf{E}_\Theta + \sin(\alpha)\mathbf{E}_Z, \tag{3.8}$$

where α, with $0 \le \alpha \le \pi/2$, is the angle that the direction makes locally with the azimuthal direction. In this situation the invariants I_4 and I_5 using (3.4) yield

$$\begin{aligned} I_4 &= (\lambda_\theta M_\Theta + \gamma\lambda_z M_Z)^2 + \lambda_z^2 M_Z^2, \\ I_5 &= \lambda_\theta^2(\lambda_\theta^2 + \gamma^2\lambda_z^2)M_\Theta^2 + 2\gamma\lambda_\theta\lambda_z(\lambda_\theta^2 + \lambda_z^2(1+\gamma^2))M_\Theta M_Z \\ &\quad + \lambda_z^2(\gamma^2\lambda_\theta^2 + (1+\gamma^2)^2\lambda_z^2)M_Z^2. \end{aligned} \tag{3.9}$$

Note that, as opposed to the case in which the fibre was in the radial direction, σ is not coaxial with $\mathbf{B}$ due to the torsion. For the circumferential transverse isotropy, i.e., $M_\Theta = 1, M_Z = 0$, the invariant I_4 does not depend on γ but I_5 depends on γ, which in turn means that the fibre length does not change with torsion. Furthermore, in general, using (3.9) it can be shown that

$$I_5 = I_4(I_1 - \lambda_\theta^{-2}\lambda_z^{-2}) - \lambda_\theta^2\lambda_z^2. \tag{3.10}$$

For positive γ, both I_4 and I_5 are monotonically increasing functions of each of γ, λ_θ and λ_z. For $\gamma < 0$ and λ_z fixed, I_4 has a minimum, which may be greater than or less than 1. The situation with I_5 is not so straightforward, and for certain values of α two minima can be found. More in particular, the invariant I_5 has two minima for $\alpha \in (\alpha_{\min}, \alpha_{\max})$ where (i) $\alpha_{\max}$ changes (slightly) with λ_z and λ_θ and (ii) $\alpha_{\min}$ tends to 0 as $\gamma \to \infty$. For $\lambda_\theta = \lambda_z = 1.2$ and $-8 < \gamma < 0$, $\alpha_{\min} \approx 3.4^\circ$ and $\alpha_{\max} \approx 15.5^\circ$ (see Fig. 2). This opens the possibility to get non-smooth solutions, whose study goes beyond this note.

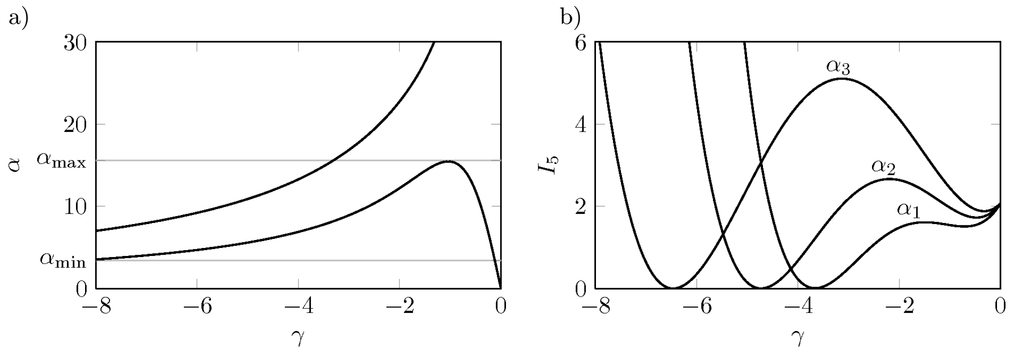

FIG. 2. The curves of (a) give the values (γ, α) obeying $\partial I_5/\partial\gamma = 0$ while the curves of (b) give the values of I_5 vs γ for $\lambda_\theta = \lambda_z = 1.2$ and $\alpha_{1,2,3} \approx 14^\circ, 11^\circ, 8^\circ$, which obey $\alpha \in (\alpha_{\min}, \alpha_{\max})$. The adimensional quantities P^*, M^* and N_r^* for values of $\alpha \in (\alpha_{\min}, \alpha_{\max})$ are similar to those corresponding to $\alpha = 0$.

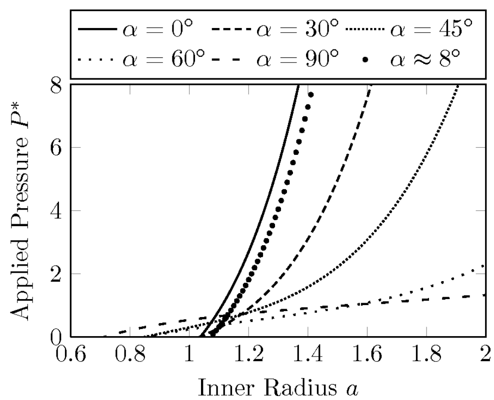

FIG. 3. The curves give the values of pressure P^* vs the inner radius a for $\tau = -0.1$ and specific values of α.

We further illustrate the results numerically for values $\rho = 2$ and $\lambda_\theta = \lambda_z = 1.2$ as well as for different values of τ and α. The qualitative behaviour of the curves in Fig. 3 is quite similar. All curves are monotonically increasing. Let us focus on the curve for which α is equal to 90°. In this case I_5 is a fixed value given by $(3.4)_2$. It follows by (3.1) that this case is qualitatively (not quantitatively) associated with the behaviour of a neo-Hookean material.

There is a correspondence between Figures 3, 4 and 5. In particular, Fig. 3 gives the values of P^* while under the same circumstances Fig. 4 gives the values of M^* and Fig. 5 gives the values of N_r^*. The plots show that curves may intersect each other which in turn means coupling among the values of the parameters involved. It is interesting to note that as the angle α decreases from 90° the

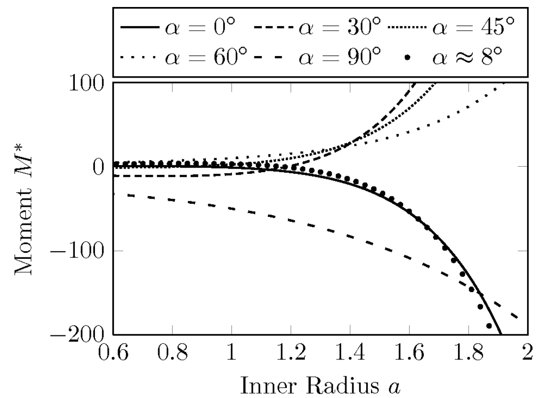

FIG. 4. The curves give the values of moment M^* vs the inner radius a for $\tau = -0.1$ and specific values of α.

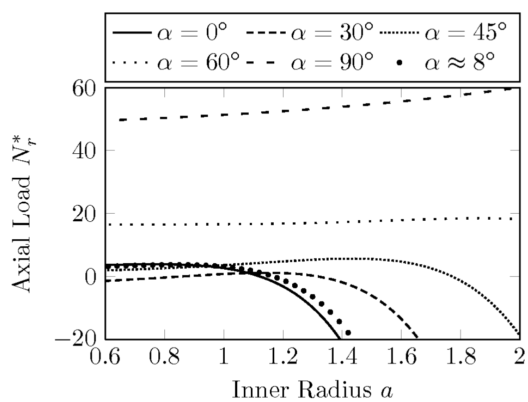

FIG. 5. The curves give the values of reduced axial load N_r^* vs the inner radius a for $\tau = -0.1$ and specific values of α.

reduced axial load in Fig. 5 turns from positive to negative as the inner radius increases.

Finally, we consider $a = 1.2$ and $\lambda_z = 1.2$ and we plot different values of the reduced load vs the torque deformation parameter τ for specific fibre angles in Fig. 6. These values are symmetric with respect to the values of the torque deformation for fibre angles $\alpha = 0$ and $\alpha = 90°$. In addition, we notice in Fig. 6 that the $\alpha = 0$-curve is associated with a range of values smaller than the range of values associated with other angles. This is due to the fact that the fibre is in the circumferential direction.

It is important to point out that the circular cylindrical configuration is maintained during loading. The quantities P^*, M^* and N_r^* are coupled and

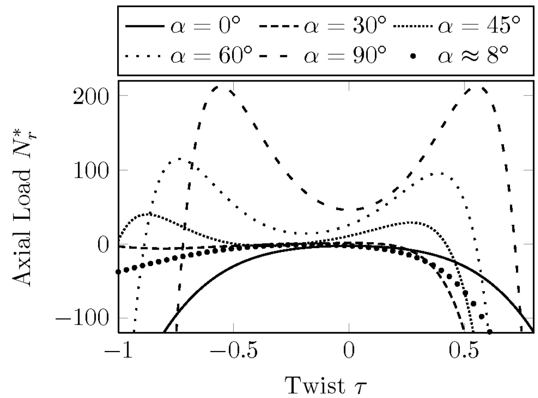

FIG. 6. Values of the reduced axial load N_r^* vs the torque deformation parameter τ for $a = 1.2$, $\lambda_z = 1.2$ and specific values of the fibre angle α.

depend on the deformation variables. Their changes with deformation give the values that make possible a cylindrical geometry.

4. Ordinary ellipticity

The loss of ordinary ellipticity was given, for instance, by [3] as

$$\mathbf{Q}(\mathbf{n})\colon \mathbf{t} \otimes \mathbf{t} = 0, \tag{4.1}$$

where

$$Q_{ij} = \mathbf{F}_{p\alpha}\mathbf{F}_{q\beta}\frac{\partial^2 W}{\partial \mathbf{F}_{j\beta}\mathbf{F}_{i\alpha}} n_p n_q$$

is the acoustic tensor and $\mathbf{t}$ and $\mathbf{n}$ are two unit vectors satisfying $\mathbf{t} \cdot \mathbf{n} = 0$. The acoustic tensor particularized for (3.1) yields

$$\begin{aligned} \mathbf{Q} = {} & 2W_1(\mathbf{B}\colon \mathbf{n}\otimes\mathbf{n})\mathbf{I} \\ & +2W_5\{2(\mathbf{B}\colon \mathbf{m}\otimes\mathbf{n})(\mathbf{m}\cdot\mathbf{n})\mathbf{I}+(\mathbf{B}\colon \mathbf{n}\otimes\mathbf{n})(\mathbf{m}\otimes\mathbf{m}) \\ & +(\mathbf{m}\cdot\mathbf{n})(\mathbf{m}\otimes\mathbf{n})\mathbf{B}+(\mathbf{m}\cdot\mathbf{n})\mathbf{B}(\mathbf{n}\otimes\mathbf{m})+(\mathbf{m}\cdot\mathbf{n})^{\mathbf{2}}\mathbf{B}\} \\ & +4W_{55}\{(\mathbf{B}\colon \mathbf{m}\otimes\mathbf{n})\mathbf{m}+(\mathbf{m}\cdot\mathbf{n})\mathbf{B}\mathbf{m}\}\otimes\{(\mathbf{B}\colon \mathbf{m}\otimes\mathbf{n})\mathbf{m}+(\mathbf{m}\cdot\mathbf{n})\mathbf{B}\mathbf{m}\}. \end{aligned} \tag{4.2}$$

The analysis of (4.1) for a given W furnishes the ellipticity status of that particular strain energy. If, for some pair of orthogonal unit vectors $\mathbf{t}$ and $\mathbf{n}$ such that $\mathbf{t} \cdot \mathbf{n} = 0$, a given deformation gradient $\mathbf{F}$ satisfies equation (4.1), then the deformation is said to be non-elliptic for that material model. Furthermore, the unit vector $\mathbf{n}$ is identified as the normal vector to a surface (in the deformed configuration), referred to as a *weak surface*, across which some of the differentiability properties required in the derivation of the equilibrium equations are not satisfied by some or all the variables involved. Once $\mathbf{F}$ is specified, it is possible to check the ellipticity of the deformation. On the other hand, using (2.14), the incompressibility constraint $\lambda_r\lambda_\theta\lambda_z = 1$, as well as (4.2) and (4.1), the ellipticity condition can be written as a function of $(\lambda_\theta, \lambda_z, \gamma, \alpha, \rho, \mu, \mathbf{n})$. One can assume that all variables are known except λ_θ and $\mathbf{n}$ and solve for those values. Whence, using (2.15), one can write $\lambda_\theta = r/\sqrt{\lambda_z(r^2 - a^2) + A^2}$ and, now, choose appropriate values for A and B to design a structure subject to elliptic deformations. Of course, this may not be possible. The following analysis sheds some light on the discussion. We consider as an example the case of radial transverse isotropy with $M_R = 1$ and assume that the unit vectors $\mathbf{t}$ and $\mathbf{n}$ are in either the rz-plane or in the $r\theta$-plane (see Fig. 7). In the former case, the two directions $\mathbf{n}$ and $\mathbf{t}$ can be written as

$$\mathbf{n} = -\sin\varphi\,\mathbf{e}_r + \cos\varphi\,\mathbf{e}_z, \qquad \mathbf{t} = \cos\varphi\,\mathbf{e}_r + \sin\varphi\,\mathbf{e}_z. \tag{4.3}$$

It follows that the condition of loss of ellipticity (4.1) does not depend on γ. The onset of ellipticity is shown for $\rho = 2$ and $\lambda_z = 1$ in Fig. 8a and $\lambda_Z = 1.2$ in Fig. 8b. The former case ($\lambda_z = 1$) corresponds to internal pressure only while the latter corresponds to combined extension and inflation. The curves in these plots obey (4.1). In Fig. 8a, ellipticity is lost for $\lambda_\theta > 1$ but very close to the undeformed configuration and the weak surface is perpendicular to the fiber

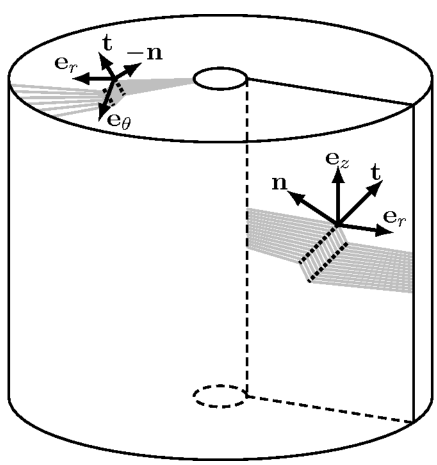

Fig. 7. Kinematics of fiber kinking in fiber reinforced materials. The boundary of the kink band in the incipient fiber kinking mechanism is interpreted as a weak surface and is close to the normal direction of the fiber reinforcement. The unit vector $\mathbf{n}$ is perpendicular to the boundary of the kink. Two possible kink bands are shown. The lower right sketch in the cylinder considers a kink band with the unit vectors $\mathbf{t}$ and $\mathbf{n}$ in the rz-plane while the upper left sketch considers a kink band with these vectors in the $r\theta$-plane.

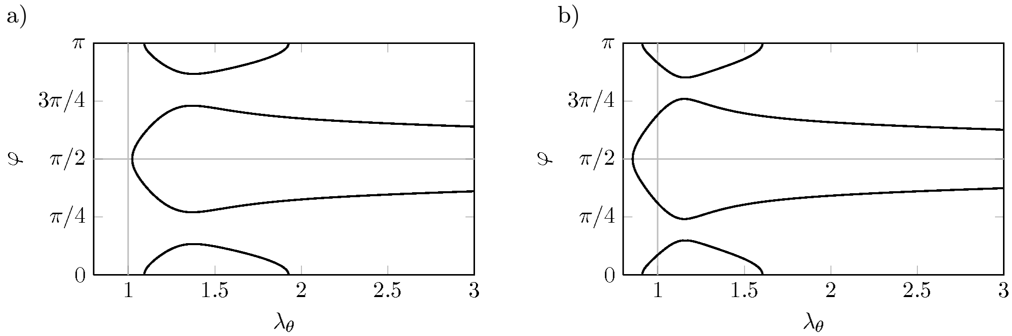

FIG. 8. The curves in these plots obey (4.1) and show the ellipticity status of a) λ_θ for $\rho = 2$ and $\lambda_z = 1$ and b) $\lambda_Z = 1.2$. The kink band is in the rz-plane.

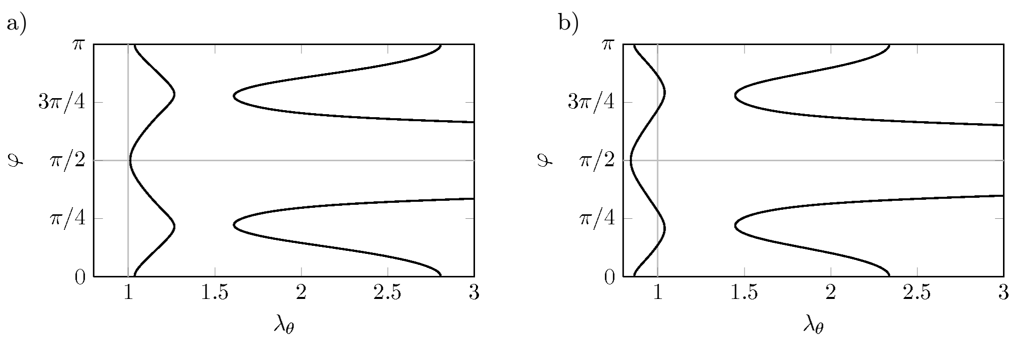

FIG. 9. The curves in these plots obey (4.1) and show the ellipticity status of a) λ_θ for $\rho = 4$ and $\lambda_z = 1$ and b) $\lambda_Z = 1.2$. The kink band is in the rz-plane.

($\varphi = \pi/2$), which is interpreted as fibre kinking. As λ_θ increases there could be two (symmetric) weak surfaces in the rz-plane: one with $\varphi > \pi/2$ and the other with $\varphi < \pi/2$. Furthermore, it is possible to obtain a weak surface parallel to the fibre obeying $\varphi = 0$, which is interpreted as fibre splitting. The description applies to the results associated with $\lambda_z = 1.2$. Whence, very moderate inflation is sufficient to lose ellipticity. Furthermore, it follows that moderate axial tensile load is just sufficient to lose ellipticity. The fibre is under compression under these circumstances. For completeness, similar plots are shown for $\rho = 4$ in Fig. 9. The two solutions that unfold in Fig. 8a (Fig. 8b), one related to fibre kinking and the other related to fiber splitting, are fully developed and emerge together in the curve on the left of Fig. 9a (Fig. 9b).

When the two directions $\mathbf{n}$ and $\mathbf{t}$ are on the $r\theta$-plane, it follows that

$$\mathbf{n} = -\sin\varphi\,\mathbf{e}_r - \cos\varphi\,\mathbf{e}_\theta, \qquad \mathbf{t} = \cos\varphi\,\mathbf{e}_r - \sin\varphi\,\mathbf{e}_\theta. \tag{4.4}$$

Under these circumstances, the loss of ellipticity condition (4.1) depends on γ.

Nevertheless, for $\gamma = 0$ results give the situation described previously with the weak surfaces now in the $r\theta$-plane.

5. Conclusions

Finite elastic deformations of a circular tube made of a fibre reinforced material subject to axial load, internal pressure and end moment has been examined. In particular, the material depends on the invariant I_5 and, to the best of our knowledge, this is one of the few papers dealing with this model. For radial transverse isotropy, the results obtained here are similar qualitatively to the ones given in [1] with regard to the invariant I_4. On the other hand, the couplings among all the variables for other directions of transverse isotropy (for instance, in certain directions perpendicular to the radial direction) give results for the model with the invariant I_5 qualitatively different to the results obtained with the model depending on the invariant I_4. In addition, we have shown that most of the deformations obtained are non-elliptic, as it is expected also for the invariant I_4. We illustrated the analysis by choosing representative values of the parameters. For other models, as well as geometries, the possibility of obtaining a wide range of non-smooth behaviour is possible.

At last, it should also be pointed out that the transversely isotropic constitutive laws at hand are not able in general to fully capture available experimental data. For instance, it has been shown by [14] that both I_4 and I_5 have to be included in the constitutive equation if the infinitesimal longitudinal and transverse shear moduli of the material are different.

Acknowledgement

The authors acknowledge support from the Ministerio de Ciencia, Spain, under the Project number DPI2011-26167. Mustapha El Hamdaoui also thanks the Ministerio de Economía y Competitividad, Spain, for funding under the Project number DPI2008-03769 and Grant number BES-2009-027812.

References

1. M. El Hamdaoui, J. Merodio, R.W. Ogden, J. Rodríguez, *Finite elastic deformations of transversely isotropic circular cylindrical tubes*, International Journal of Solids and Structures, **51**, 5, 1188–1196, 2014.
2. J. Merodio, R.W. Ogden, *Remarks on instabilities and ellipticity for a fiber-reinforced compressible nonlinearly elastic solid under plane deformation*, Quarterly of Applied Mathematics, **63**, 2, 325–333, 2005.
3. J. Merodio, P. Neff, *A note on tensile instabilities and loss of ellipticity for a fiber-reinforced nonlinearly elastic solid*, Archives of Mechanics, **58**, 3, 293–303, 2006.

4. J. Merodio, R.W. Ogden, *Tensile instabilities and ellipticity in fiber-reinforced compressible non-linearly elastic solids*, International Journal of Engineering Science, **43**, 89, 697–706, 2005.

5. S.H Lee, C.S. Yerramalli, A.M Waas, *Compressive splitting response of glass-fiber reinforced unidirectional composites* Composites Science and Technology, **60**, 16, 2957–2966, 2000.

6. R.S. Rivlin, D.W. Saunders, *Large elastic deformations of isotropic materials. VII: experiments on the deformation of rubber*, **243**, 865, 251–288, 1951.

7. A.N. Gent, R.S. Rivlin, *Experiments on the mechanics of rubber, II: The torsion, inflation and extension of a tube*, Proceedings of the Physical Society. Section B, **65**, 7, 487, 1952.

8. L. Kanner, C. Horgan, *On extension and torsion of strain-stiffening rubber-like elastic circular cylinders*, Journal of Elasticity, **93**, 1, 39–61, 2008.

9. C. Horgan, D. Polignone, *A note on the pure torsion of a circular cylinder for a compressible nonlinearly elastic material with nonconvex strain-energy*, Journal of Elasticity, **37**, 2, 167–178, 1994.

10. D.M. Haughton, R.W. Ogden, *Bifurcation of inflated circular cylinders of elastic material under axial loading. Mmbrane theory for thin-walled tubes*, Journal of the Mechanics and Physics of Solids, **27**, 3, 179–212, 1979.

11. J. Merodio, D.M. Haughton, *Bifurcation of thick-walled cylindrical shells and the mechanical response of arterial tissue affected by marfans syndrome*, Mechanics Research Communications, **37**, 1, 1–6, 2010.

12. J. Rodríguez, J. Merodio, *A new derivation of the bifurcation conditions of inflated cylindrical membranes of elastic material under axial loading. Application to aneurysm formation*, Mechanics Research Communications, **38**, 3, 203–210, 2011.

13. J. Merodio, R.W. Ogden, *Mechanical response of fiber-reinforced incompressible non-linearly elastic solids*, International Journal of Non-Linear Mechanics, **40**, 23, 213–227, 2005.

14. J.G. Murphy, *Transversely isotropic biological, soft tissue must be modelled using both anisotropic invariants*, European Journal of Mechanics - A/Solids, **42**, 90–96, 2013.

Received March 19, 2014; revised version August 4, 2014.